International Journal of Climatology

International Journal of Climatology | RMetS

RESEARCH ARTICLE

A Study of Recent Changes in Moisture Flux Patterns Over India: Implications for Indian Summer Monsoon Rainfall

Amarjeet[1] | Vasubandhu Misra[2,3] | Arun Chakraborty[1] | Anil K. Gupta[4] | Vineet Sharma[1]

[1]Centre for Ocean, River, Atmosphere and Land Sciences (CORAL), Indian Institute of Technology Kharagpur, Kharagpur, West Bengal, India | [2]Center for Ocean-Atmospheric Prediction Studies (COAPS), Florida State University, Tallahassee, Florida, USA | [3]Department of Earth, Ocean and Atmospheric Science, Florida State University, Tallahassee, Florida, USA | [4]Department of Geology and Geophysics, Indian Institute of Technology Kharagpur, Kharagpur, West Bengal, India

Correspondence: Arun Chakraborty (arunc@coral.iitkgp.ac.in)

Received: 4 October 2024 | **Revised:** 26 May 2025 | **Accepted:** 29 May 2025

Funding: This work was supported by the Anusandhan National Research Foundation (ANRF), New Delhi, under the J.C. Bose Fellowship (Grant JBR/2021/000019) and Indian Institute of Tropical Meteorology Pune, Ministry of Earth Sciences, Government of India to conduct this research under Monsoon Mission III (Grant IITM/MM-III/2024/AI-P06/SO-006).

Keywords: Indian summer monsoon rainfall | moisture flux | moisture source and sink | moisture transport | precipitable water content

ABSTRACT

This study examines the changes in the linear trends of the precipitable water content (PWC) associated with the Indian summer monsoon rainfall using the ERA-5 datasets. The study period of 63 years (1959–2021) is divided into two time periods P1: 1959–2001 and P2: 2002–2021. In the recent period (P2), we observe a significant rise in the statistically significant linear trend of the mean JJAS PWC leading to a significant positive difference of P2 − P1 over most of India. This change is found to be largest in the middle troposphere, where the rotational component of the moisture flux is strengthened in P2 relative to P1. This modulation is attributed to the non-uniform rate of change of tropospheric air temperature in the lower and middle troposphere in P2 from the rising land–ocean thermal contrast. This results in stabilising the atmosphere. Consequently, we also observe an increase in the fraction of stratiform precipitation in P2 relative to P1. This increase in stratiform precipitation is associated with enhanced mid-atmospheric diabatic heating and mid-tropospheric southwesterly moisture flux, which enhances PWC in P2 compared to P1.

1 | Introduction

The Indian summer monsoon rainfall (ISMR) is crucial to meet the agricultural and domestic water demand and to replenish the groundwater reservoirs (Asoka et al. 2017; Gadgil et al. 1999). The Indian summer monsoon (ISM) system accounts for 80% of the total rainfall in India (Bollasina et al. 2014; Mooley and Parthasarathy 1984). The analysis of moisture flux and its variations to understand the changing rainfall patterns is necessary, given the significant influence of moisture flux and precipitable water on ISM (Misra et al. 2012; Trenberth et al. 2005). In the context of ISM, the associated variation in precipitable water, moisture flux and its divergence (source) and convergence (sink) have been studied by numerous researchers (Chakraborty et al. 2006; Jin and Wang 2017; Ratna et al. 2014; Roxy et al. 2017; Ruprecht and Kahl 2003; Trenberth et al. 2005; Ullah and Gao 2012). In this study, we intend to examine the variations of the ISMR by splitting the moisture flux vector into its rotational and divergent components (DCs), which inform on the moisture transport and its source/sink, respectively. This analysis will be conducted over the Indian homogeneous rainfall regions (IHRRs; Figure S1), which are so designated by similarities in their rainfall features following Parthasarathy et al. (1996).

Several studies have been carried out to explain the relationship between moisture and rainfall over the Indian region. For example, using backward trajectories, Pathak et al. (2017) identified

20 terrestrial and seven oceanic moisture sources for the precipitation over the Indian landmass using the ERA-I data and a Dynamic Recycling Model. They reported a maximum and continuous moisture contribution for ISMR from the western, central, northern Indian Ocean, Ganga River Basin (maximum terrestrial moisture contributor) and the Red Sea including the neighbouring gulf. However, cross-equatorial moisture sources related to ISMR have also been reported to be important in Ramesh Kumar et al. (1999). Similarly, Roxy (2017) also indicate the role of excess moisture supply through low-level jets from the Arabian Sea, which sometimes contribute to a threefold rise in extreme rainfall events in central India (CI). Likewise, Kumari et al. (2022) showed that low-level jet is the dominating factor for very high rainfall events, while the availability of convective available potential energy plays a vital role in light rain events. They also indicated a decrease and an increase in the frequency of light and heavy to extreme rainfall events in the period from 1951 to 2015, respectively. However, local moisture recycling also plays a vital role in sustaining the ISMR for extended periods (Pathak et al. 2014).

A few studies also reported an increase in the mean ISMR trend during the initial decades of the 21st century (Jin and Wang 2017; Ratna et al. 2014). Ratna et al. (2014) have linked the recent increase in mean ISMR to rising atmospheric moisture levels over the Arabian Sea. This is believed to be a result of higher SST during the period of 2003–2012 compared to the previous decade (1993–2002). They suggest that the increased moisture supply from the Arabian Sea to the Indian mainland during this time frame led to a relative increase in precipitation over India in the 2003–2012 period relative to 1993–2002. Similarly, using multiple observational datasets, Jin and Wang (2017) showed a positive trend of ISMR of $1.34\,\mathrm{mm\,day^{-1}\,decade^{-1}}$ since 2002. They attributed this rising trend to the increasing land–ocean temperature gradient. In a review article, Singh et al. (2019) indicate that a growing consensus from modelling studies of the ISM is that the ISM will intensify by the end of the 21st century due to an increase in moisture convergence despite a weakening of the monsoon circulation.

This study investigates the variations in the seasonal mean precipitable water content (PWC) over the ISMR region in recent decades compared to previous decades, offering an explanation for the corresponding changes. Some studies have shown a recent increase in PWC in both terms of trends and climatology on different spatial–temporal scales (Krishnan et al. 2025; Sarkar et al. 2023; Tomar et al. 2024), which, however, do not provide any idea regarding the possible mechanism behind this change, rather giving a single argument of global warming. In our approach, we tried to provide a possible mechanism for how the recent non-symmetric tropospheric warming results in a strengthened rotational component (RC) of moisture flux, which causes more moisture incursion over the region, especially in the middle layer of the troposphere. Hence, the novelty of our study stems from the fact that we provide the dynamical mechanism of how the PWC is increasing over time and space. These changes to the PWC of the ISMR with the possible mechanism have, heretofore, not been reported elsewhere. The analysis will focus on the mean changes in moisture transport, as well as the sources and sinks of moisture, across these multi-decadal periods. Additionally, the study will explore the changes in the distribution of convective and stratiform precipitation during these periods. The analysis consequently provides a unique perspective to long-term changes in ISM. In the following section, we describe the data and methodology, followed by a discussion of results in Section 3 and conclusions in Section 4.

2 | Data and Methodology

The European Centre for Medium-Range Weather Forecast's (ECMWF's) advanced ERA-5 atmospheric reanalysis (Hersbach et al. 2019) has been used for the following variables: specific humidity (q), zonal (u) and meridional (v) components of wind, tropospheric air temperature, total, convective and stratiform precipitation. The monthly rainfall data are obtained from the India Meteorological Department (IMD; Kishore et al. 2016). Several studies have used these datasets to study the ISM and other weather-associated phenomena (Kumar et al. 2023; Sharma et al. 2024). Both datasets have a finer resolution of $0.25° \times 0.25°$ from 1959 to 2021 with monthly averaged values. The entire study period has been divided into two periods: P1 (1959–2001) and P2 (2002–2021). Many studies have acknowledged 2002 to be a change point in the linear trends of the ISMR (Amarjeet et al. 2023; Jin and Wang 2017; Ratna et al. 2014).

Given the associated uncertainties of the moisture analysis in the reanalyses (Bengtsson et al. 2004; Trenberth et al. 2011), we have examined the fidelity of PWC in ERA-5 relative to sonde data from 19 locations (Figure S1; Table S1) over India using the Integrated Global Radiosonde Archive (IGRA) version 2.0 provided by National Centers for Environmental Information (NCEI-NOAA; Durre et al. 2006, 2018). In Figure S2, the mean JJAS PWC from ERA-5 shows a good correspondence with the IGRA dataset. However, there is a general underestimation of PWC in ERA-5 relative to IGRA, with the largest dry bias in the last 3 years of 2019, 2020, and 2021. This verification provides a reasonable justification for using the PWC of ERA-5 for the study of the ISM.

The study has been carried out only for two seasons: the pre-monsoon season of March–April–May (MAM) and the monsoon season of June–July–August–September (JJAS). The pre-monsoon season is included to show the seasonality of the reported change. Figure S1 shows the IHHRs following Parthasarathy et al. (1996), which are north-western India (NWI), central north-eastern India (CNEI), north-eastern India (NEI), CI and peninsular India (PNI).

The PWC, rotational (ψ) and divergent (χ) components of the moisture flux are calculated following Chakraborty et al. (2006).

$$\mathrm{PWC} = \frac{1}{g}\int_{P_t}^{P_s} q\, dp \tag{1}$$

We calculate the zonal (u) and the meridional (v) components of moisture flux as:

$$Q_u = \frac{1}{g}\int_{P_t}^{P_s} qu\, dp \text{ and } Q_v = \frac{1}{g}\int_{P_t}^{P_s} qv\, dp \tag{2}$$

where, $\boldsymbol{Q} = Q_u \cdot \hat{\imath} + Q_v \cdot \hat{\jmath}$. Moisture flux vectors, $\boldsymbol{Q}$ is further decomposed into its rotational and DCs (Rosen et al. 1979) by writing in terms of stream function (ψ) and velocity potential (χ):

$$\boldsymbol{Q} = \hat{k} \times \nabla\psi + \nabla\chi \tag{3}$$

$$\nabla^2\psi = \hat{k} \cdot \nabla \times \boldsymbol{Q} \text{ and } \nabla^2\chi = \nabla \cdot \boldsymbol{Q} \tag{4}$$

The rotational and DC of moisture flux is calculated from Equation (4) using the spectral method (Krishnamurti et al. 2006). The Helmholtz decomposition using the spectral method entails using Legendre polynomials in the meridional and Fourier decomposition in the zonal direction as basic functions to solve for the irrotational ($\vec{Q}^d$) and non-divergent ($\vec{Q}^r$) moisture flux vectors (Haltiner and Williams 1980). The irrotational ($\vec{Q}^d$) and non-divergent ($\vec{Q}^r$) moisture flux vectors are calculated from χ and ψ, respectively as:

$$Q_u^r = -\frac{d\psi}{dy}, Q_v^r = \frac{d\psi}{dx} \text{ and } Q_u^d = \frac{d\chi}{dx}, Q_v^d = \frac{d\chi}{dy} \tag{5}$$

where q is specific humidity; g is the acceleration due to gravity; u and v are zonal and meridional wind components, respectively; P_s is the pressure at the bottom of the air column; P_t, pressure at the top of the air column.

The equation used to calculate the rate of heating due to the apparent heat source Q_1 is derived from Yanai et al. (1973):

$$\frac{Q_1}{C_p} = \frac{\partial\overline{T}}{\partial t} + \overline{\boldsymbol{V}\cdot\nabla T} + \frac{\overline{\omega}}{C_p}\frac{\partial\overline{s}}{\partial p} \tag{6}$$

where C_p is the specific heat at constant pressure; T is air temperature; $\boldsymbol{V}$ is the horizontal wind vector; ω is vertical p-velocity; and s is dry static energy. The bar shows the horizontal averages.

The non-divergent or RC represents moisture transport, while the irrotational or DC emphasises the source or sink region of the moisture. The linear trend analyses are performed using the Mann–Kendall significance test (Hirsch and Slack 1984). We investigate the moisture flux over different vertical atmospheric layers of the IHRRs following Chakraborty et al. (2006). Therefore, we have divided the troposphere vertically into three layers: lower (1000–850 hPa), middle (850–500 hPa) and upper (500–100 hPa) troposphere.

3 | Results

3.1 | Temporal and Spatial Variation in PWC

The time series of all India averaged PWC in Figure 1 for the JJAS season shows very clearly that 2002 serves as a change point in their linear trends. JJAS shows a weak, statistically insignificant negative trend (−0.014 mm/decade) in P1, which changes to a statistically significant positive trend of 2.2 mm/decade in P2 (Figure 1). A similar feature in the trends of all India averaged annual mean PWC is also seen with the year 2002 appearing as the change point when the time series spans across all seasons of the year (Figure S3). Similarly, these features of the linear trends of PWC over India are also observed in the March–April–May (Figure S4a), October–November–December (Figure S4b) and January–February (Figure S4c) seasons, albeit with different slopes and statistical significance. In the rest of the paper, however, we will focus on the JJAS season, which conforms to the ISM.

The year 2002 has been viewed as a change point of the ISM in previous studies (e.g., Amarjeet et al. 2023; Jin and Wang 2017; Ratna et al. 2014). We also tracked the rolling decadal trends of the mean JJAS PWC starting out from each year of 1959–2010 (Figure S5), which shows a gradually rising trend to reach 2.2 mm/decade by 2002, after which the decadal trends begin to vary significantly. Similarly, we also computed linear trends of the mean JJAS PWC in segments of 20 years (Figure S6). The last 20-year segment, corresponding to 2002–2021, showed a statistically significant trend of 2.2 mm/decade at a 1% significance level relative to statistically insignificant trends in the other two segments (Figure S6).

The spatial patterns of these linear trends of PWC in Figure 2 show an extensive change across India. During P2, a significant positive trend ranging between 1.2 and 3.6 mm/decade develops over most of India in JJAS, except in the hilly regions and the north-western edge of NWI (Figure 2b), which is in contrast to insignificant trends over most of India in P1 (Figure 2a).

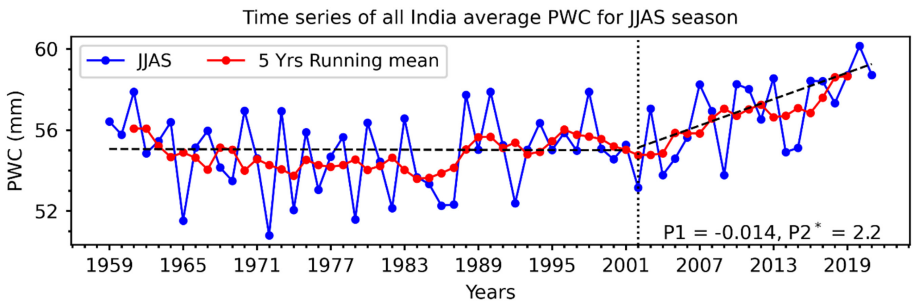

FIGURE 1 | Time series of all India average of PWC in JJAS season. The legend indicates the slopes of the trends in mm/decade for P1 and P2, where * shows significance at 10% significance level following the Mann–Kendall test. The red and black (dashed) lines show the 5-year running mean and slope of the trends, respectively. [Colour figure can be viewed at wileyonlinelibrary.com]

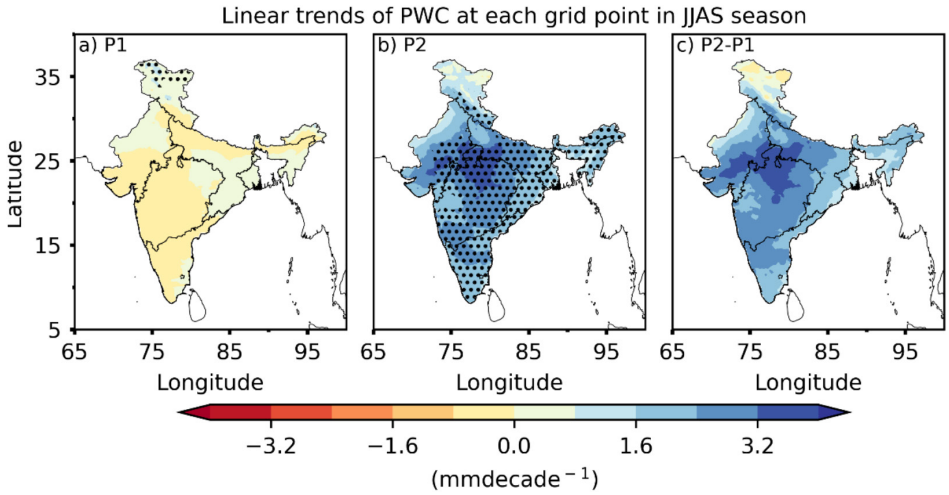

FIGURE 2 | The linear trends of mean JJAS PWC at each grid point during (a) P1, (b) P2 and (c) P2 − P1 periods. The stippled regions show significance at the 5% significance level following the Mann-Kendall test. [Colour figure can be viewed at wileyonlinelibrary.com]

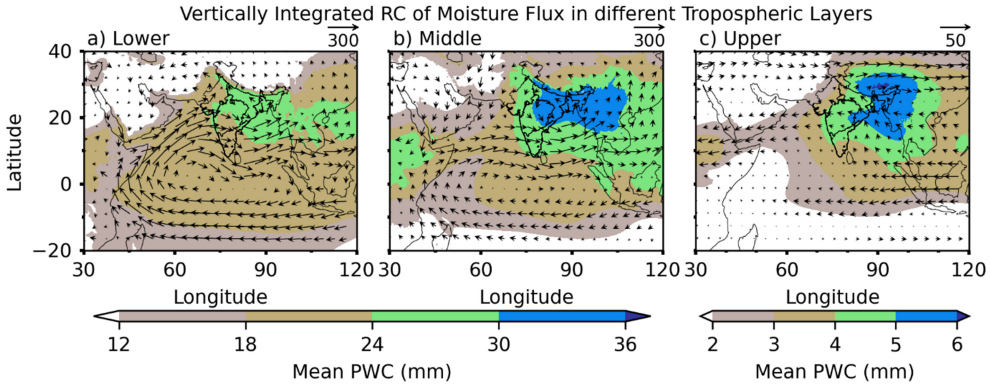

FIGURE 3 | The climatological JJAS PWC (shaded; unit: mm) overlaid with the rotational component (RC) of moisture flux (vectors; unit: $kgm^{-1}s^{-1}$) for (a) lower (1000–850 hPa), (b) middle (850–500 hPa) and (c) upper (500–100 hPa) layers of the troposphere. [Colour figure can be viewed at wileyonlinelibrary.com]

3.2 | Rotational Component (RC) of Moisture Flux

The seasonal climatology of the RC of moisture flux in the various atmospheric layers is analysed separately over the ISM region (including IHRRs) for the entire period including P1 and P2. Figure 3 illustrates the PWC (integrated over the three atmospheric layers separately), which shows more PWC in the lower and middle troposphere while far less in the upper troposphere. In JJAS, over the IHRRs, the PWC varies up to and over 36 mm in the lower to middle troposphere (Figure 3a,b). The cross-equatorial southwesterly RC of the moisture flux is apparent in the lower (Figure 3a) and middle (Figure 3b) troposphere. A notable feature is the cyclonic RC of the moisture flux vectors over the NEI region in Figure 3a–c. This coincides with the climatological monsoon trough, which results in significant moisture incursion in the region, leading to a PWC maximum. It is also interesting to note that the PWC is higher in the middle troposphere (Figure 3b) compared to the lower troposphere (Figure 3a).

The changes in the seasonal mean PWC between periods P2 and P1 (shown in Figures 1 and 2) are further explained in Figure 4, which illustrates the changes in PWC and RC of the moisture flux across the different atmospheric layers. The change in PWC is largely positive, with the largest and smallest changes in the middle (Figure 4b) and the upper (Figure 4c) troposphere, respectively. However, this change is not confined to the IHRRs only but is also observed across the South Asia region, which consists of the surrounding ocean and the neighbouring countries of India. The vertical variation of the change in PWC is, however, not uniform. In the lower layers, this change in PWC is maximum over NWI and the surrounding regions, including parts of the Arabian Peninsula, supported by a strengthened southwesterly flank of RC of moisture flux from the Arabian Sea and southeasterly flow from the Bay of Bengal that transports more moisture towards NWI (Figure 4a).

Interestingly, the changes in PWC and RC of moisture flux are largest in the middle troposphere during JJAS (Figure 4). In the middle troposphere, an increased accumulation of PWC is apparent over IHRRs (with a maximum over NWI). In fact, this increase spans from the Bay of Bengal to parts of the Arabian Sea and the equatorial Indian Ocean (Figure 4b). This recent decade's relative increase of PWC in the middle troposphere is associated with the corresponding strengthening of the RC of moisture flux in P2 during JJAS. The latter strengthening reflects the increased moisture incursion over the Indian land mass and the nearby regions in the recent decades in the middle troposphere (Figure 4b),

which exceeds the corresponding change in the lower troposphere (Figure 4a). Our finding of increased PWC in recent decades corroborates similar findings of Patel and Kuttippurath (2022). They suggested that a higher evaporation rate from warming surrounding oceans, along with higher surface air temperature over land that enhanced the land–ocean contrast, led to increased PWC over India in recent decades.

3.3 | Variation in Tropospheric Air Temperature

This enhanced PWC in the lower and middle troposphere follows previous studies, which reported strengthening of the westerlies, attributed to the strengthening of the land–ocean thermal contrast (Jin and Wang 2017; Ratna et al. 2014; Roxy et al. 2017). In this study, we are interested in examining the vertical variations in these changes between the two epochs. We aim to look into the recent changes (P2 – P1) in the tropospheric temperature during MAM (Figure S7) and JJAS (Figure 5) seasons at several pressure levels between 1000 and 500 hPa to understand the reason for the unequal change of PWC in the lower (less) and middle (more) troposphere. During the pre-monsoon season of MAM, we observe intense warming for the majority of the study region except over most of India at 800, 900 and 1000 hPa, which exhibit cooling in P2 relative to P1 (Figure S7a–c). This cooling over the Indian landmass weakens the land–ocean thermal contrast. This could be a potential reason for diverting the lower troposphere RC of moisture flux towards the North-western part of India and Pakistan, where relatively stronger land surface warming is seen. However, a relatively uniform warming across the domain is observed at 700–500 hPa (Figure S7d–f).

We similarly examined the difference for P2 – P1 for JJAS in Figure 5. We found statistically significant changes in each

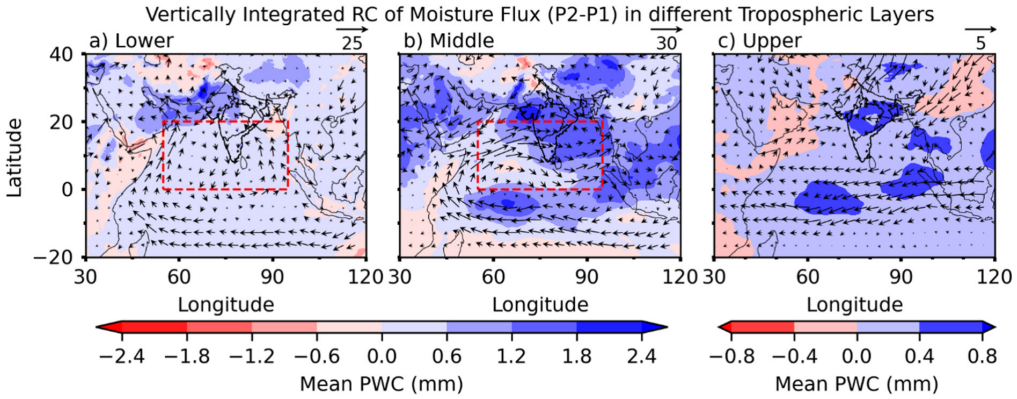

FIGURE 4 | The climatological mean JJAS change (P2 – P1) of PWC (shaded; unit: mm) overlaid with the rotational component (RC) of moisture flux (vectors; unit: $kgm^{-1}s^{-1}$) for (a) lower (1000–850 hPa), (b) middle (850–500 hPa) and (c) upper (500–100 hPa) layers of the troposphere. The red rectangle shows the region selected to study the linear changes in zonal RC of the moisture flux, explained in Section 3.3. [Colour figure can be viewed at wileyonlinelibrary.com]

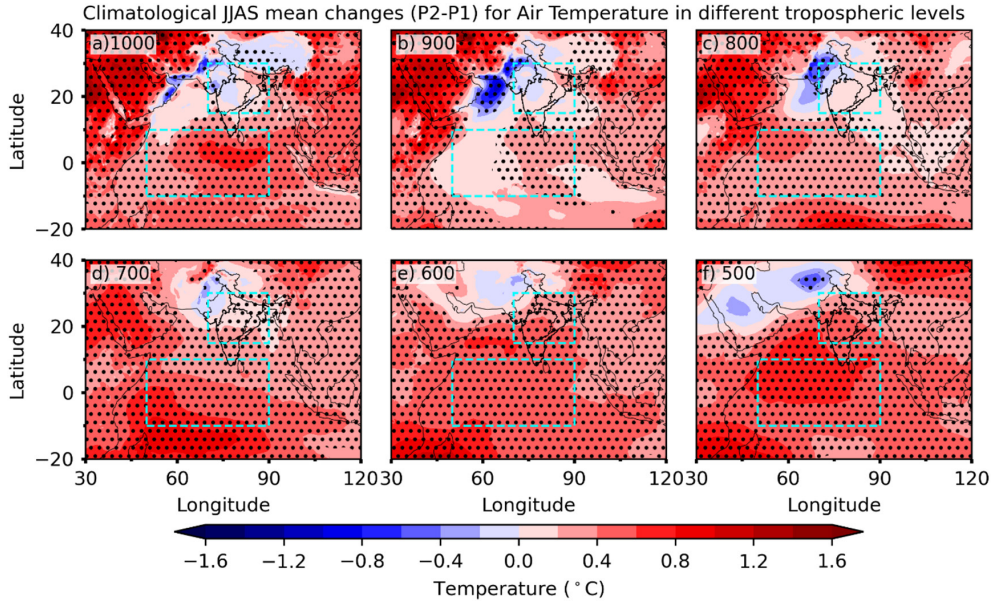

FIGURE 5 | Seasonal mean JJAS climatological change (P2 – P1) in tropospheric air temperature at (a) 1000, (b) 900, (c) 800, (d) 700, (e) 600 and (f) 500 hPa. The stippled regions show significance at a 5% significance level following the Student's *t*-test. The cyan rectangles show the regions selected to study the thermal contrast between land and ocean. [Colour figure can be viewed at wileyonlinelibrary.com]

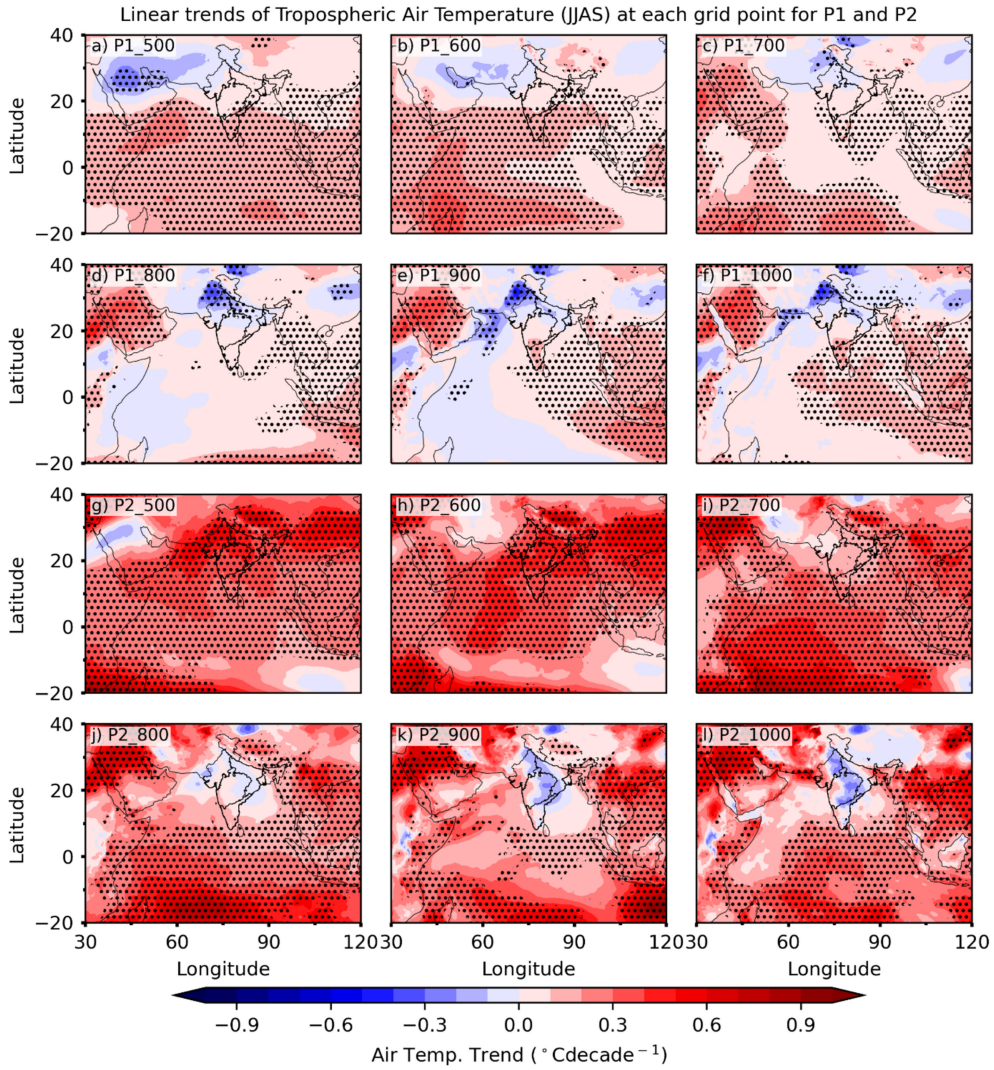

FIGURE 6 | The linear trend of mean JJAS tropospheric air temperature at each grid point at (a and g) 500 hPa, (b and h) 600 hPa, (c and i) 700 hPa, (d and j) 800 hPa, (e and k) 900, and (f and l) 1000 hPa for (a–f) P1 and (g–l) P2 periods. The stippled regions indicate significance at the 5% significance level according to the Mann–Kendall test. [Colour figure can be viewed at wileyonlinelibrary.com]

level from 1000 to 500 hPa, but with a uniform positive change in air temperature over land and ocean in 500 and 600 hPa only (Figure 5d,e). At lower levels or higher pressure levels (800–1000 hPa), similar to MAM, cooling is observed (albeit largely insignificant) over the Indian region, with a maximum over NWI and the neighbouring areas. However, this cooling pattern extends up to 500 hPa in regions northwest of India (Figure 5a–f). It is evident from Figures S7 and 5 that in recent decades, over the Indian region, there has been cooling in the lower troposphere, while over the ocean, a warming condition has prevailed. Furthermore, we have shown that compared to the middle troposphere (850–500 hPa), the lower troposphere (1000–850 hPa) change in PWC is much less in recent decades (Figure 4a,b). Such non-uniform PWC changes might be attributable to non-uniform changes in the air temperature at different pressure levels.

To further examine these changes, we have computed the tropospheric air temperature linear trends at each grid point for the two epochs (P1 and P2) for both seasons (MAM and JJAS) and at all six pressure levels between 1000 and 500 hPa (Figures S8 and 6). The temperature trends in the two epochs for MAM are significantly different (Figure S8). The P1 period displays a relatively weak cooling rate of up to −0.3°C/decade from 1000 to 700 hPa (Figure S8c–f). In contrast, P2 shows significantly enhanced cooling rates (−0.6°C to −0.9°C/decade from 1000 to 500 hPa) and a larger spatial extent covering the whole Indian subcontinent except PNI (Figure S8g–l). The warming rates over the surrounding oceans and the tropical Indian Ocean in MAM have, however, significantly strengthened in P2 compared to P1. These pre-monsoonal cooling rates over land and warming over the ocean could potentially affect the evolution of the JJAS monsoon and its overall intensity (Roxy et al. 2015).

Similarly, Figure 6 shows the JJAS tropospheric temperature linear trends for the same pressure levels as in Figure S8. In P1, a weak cooling rate is visible over the northern Indian subcontinent in 1000–700 hPa levels (Figure 6c–f), while in 600 and 500 hPa (Figure 6a,b), it shifts further west. Notably, the temperature trends in P1 over CI and PNI are positive at all levels during P1, which may indicate a slightly favourable condition of land–ocean thermal contrast for the ISM evolution in

P1. In contrast to P1, P2 shows a drastic change in these trends with slopes > 0.3°C/decade over both land and oceanic regions at all pressure levels above 800 hPa (Figure 6g–i). In the lower levels, over the Indian landmass, the trends exhibit a negative slope during P2 period (Figure 6j–l). Interestingly, the 500–600 hPa levels show higher warming rates over land regions than the ocean (Figure 6g,h). This temperature trend changes between the two epochs could affect the monsoon strength by altering the thermal contrast between land (15° N–30° N, 70° E–90° E) and ocean (10° S–10° N, 50° E–90° E). These regions are outlined in Figure 5. Roxy (2017) indicates that a warmer land than the ocean strengthens the monsoon by strengthening the thermal contrast between land and ocean. The monsoonal winds (westerlies) maximally supply moisture from the west to east direction in the mean, which occurs by the zonal component (u). Since we are using RC of moisture flux to study water transport, we consider its zonal part $\left(Q_u^r\right)$ as the primary contributor to moisture incursion during ISM season. The region for calculating Q_u^r is outlined in Figure 4 and covers a domain of 0° N–20° N and 55° E–95° E. This region is chosen based on the maximum westerly component of the moisture flux passing over India. Beyond 20° N, these monsoonal winds turn into south-easterlies as part of the monsoon trough over the Indo-Gangetic Plain. Thus, we selected this region only to investigate the changes in westerlies.

Figure S9a,b illustrate the time series of the vertically integrated Q_u^r in the lower (1000–850 hPa) and middle (850–500 hPa) troposphere with thermal contrast (computed over the boxes) outlined in Figure 5 of the lower (900, 1000 hPa) and middle (500, 600, 700 and 800 hPa) levels of the troposphere. The corresponding correlations of the thermal contrast at the various pressure levels with the RC of moisture flux from Figure S9 are indicated in Table 1. The positive correlations in Table 1 for period P1 at 500 and 600 hPa suggest that the warming or cooling of land relative to the ocean increases or decreases the RC of the moisture flux in the area outlined in Figure 4, respectively. It may be noted that the land–ocean contrast in reference to the ISM is strongest in the middle and upper troposphere owing to the upper-level heat source of the Tibetan Plateau (Noska and Misra 2016; Yanai et al. 1992). But in this period of P1, the temperature trend at these pressure levels is that of cooling over northern India while the ocean is warming (Figure 6a,b), which weakens this contrast and would, therefore, reduce the RC component of the moisture flux. Conversely, in the P2 period, these pressure levels exhibit a warming trend (Figure 6g,h) that would increase the contrast and increase the RC of the moisture flux. However, the relationship between RC of the moisture flux and the thermal contrast weakens in the mid-troposphere in P2 relative to P1.

TABLE 1 | Correlation analysis of different tropospheric level's land–ocean thermal contrast (TC) with zonal (Q_u^r) part of the rotational component (RC) of moisture flux for the middle (500–800 hPa) and lower (900–1000 hPa) levels of the troposphere.

TC levels (hPa)	Q_u^r (middle layers)		Q_u^r (lower layers)	
	P1	P2	P1	P2
500	0.71***	0.45**	—	—
600	0.47***	0.27	—	—
700	−0.14	−0.15	—	—
800	−0.50***	−0.23	—	—
900	—	—	−0.44***	0.16
1000	—	—	−0.39***	0.12

Note: Here, the middle and lower layers represent the vertically integrated values of RC across 850–500 and 1000–850 hPa, respectively.
*** and ** show significance at 1% and 5% significance levels following the Mann–Kendall test, respectively.

In Figure 7a, we show the linear trends of the mean JJAS all India averaged stratiform precipitation for the two epochs. They are significantly different in the two periods, with a decreasing trend in P1 at $-0.16\,\mathrm{mm\,day^{-1}\,decade^{-1}}$ while a rising trend of $0.3\,\mathrm{mm\,day^{-1}\,decade^{-1}}$ is observed for P2. In both these, significant. This rising trend in P2 could be a result of the corresponding stabilisation of the atmospheric lapse rate from the warming of the mid-troposphere seen earlier (Figure 6g,h). The spatial distribution of the linear trends for stratiform precipitation for P1 in Figure 7b indicates that the decrease is widespread across India and the surrounding oceans. However, in P2, there is a drastic change with the rising trend over most of India and the surrounding oceans except for some of the hilly regions of India (Figure 7c,d). These changes to the fraction of stratiform precipitation in the ISMR have a huge implication for the mid-troposphere circulation of the ISM (Choudhury and Krishnan 2011). Stratiform precipitation has a unique latent heating profile with maximum heating at a lower pressure level than deep convective heating and also has a characteristic cooling in the lower troposphere (Houze Jr 2004; Mapes 1993; Schumacher et al. 2004). In a set of idealised modelling experiments, Choudhury and Krishnan (2011) show that changes in the fraction of stratiform and convective rainfall in ISMR have a profound influence on the mid-tropospheric flow of the ISM, which is spatially very extensive. This is a result of the forced Rossby wave response that disperses westward from the monsoon trough, a major source of the latent heating at mid-levels from stratiform precipitation of the ISMR. These findings are consistent with earlier studies which indicate that the elevated vertical gradient of heating from stratiform precipitation is more effective in strengthening the upper tropospheric response of the tropical Walker and Hadley circulations as compared to deep convective precipitation with a single peak in the mid-troposphere (Mapes 1993; Schumacher et al. 2004). We, therefore, suggest that in addition to the increased land–ocean thermal contrast, the enhanced RC of the moisture flux seen in the mid-troposphere in P2 relative to P1 in Figure 4e is also a result of the enhanced stratiform precipitation in P2. These conclusions are justified from the changes in the diabatic heating (Q_1 following Yanai et al. 1973) profile shown in Figure 8a, wherein, P2 shows enhanced mid-tropospheric heating compared to P1 period. Furthermore, we also see differences in the diabatic heating between P2 and P1 in the mid-tropospheric pressure levels in Figure 8b–f, which clearly indicate an increase in the latter period over most of peninsular and western India. In Figures S10 and S11, we show similar panels as in Figure 7 for convective and total precipitation, respectively. The decreasing trends of the convective precipitation over the Arabian Sea, Bay of Bengal and NEI in P2 are significant, while over PNI,

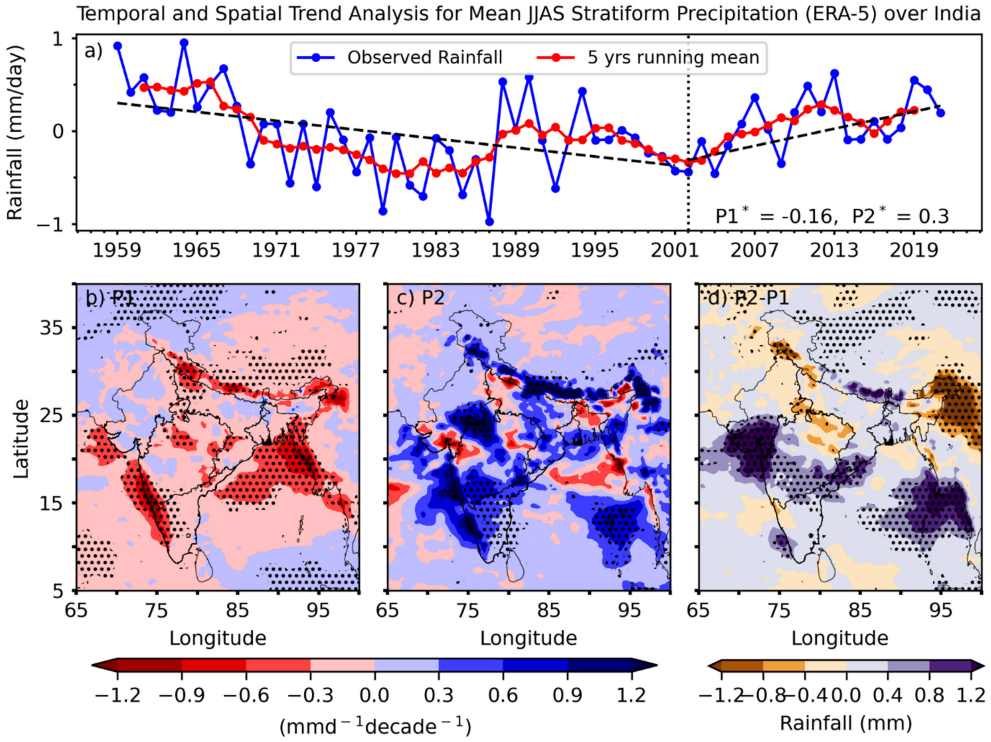

FIGURE 7 | (a) Time series of the mean JJAS all India averaged stratiform precipitation from ERA5 with the legend indicating the slopes of the trends for P1 and P2 in mm day^{-1} decade^{-1}, where * shows significance at 5% significance level following the Mann–Kendall test. The red and black (dashed) lines show the 5-year running mean and slope of the trends, respectively. The spatial distribution of the linear trends of mean JJAS stratiform precipitation from ERA5 for (b) P1 and (c) P2, and (d) the corresponding differences P2 − P1. The stippled regions indicate significance at 5% significance level according to the Mann–Kendall test. [Colour figure can be viewed at wileyonlinelibrary.com]

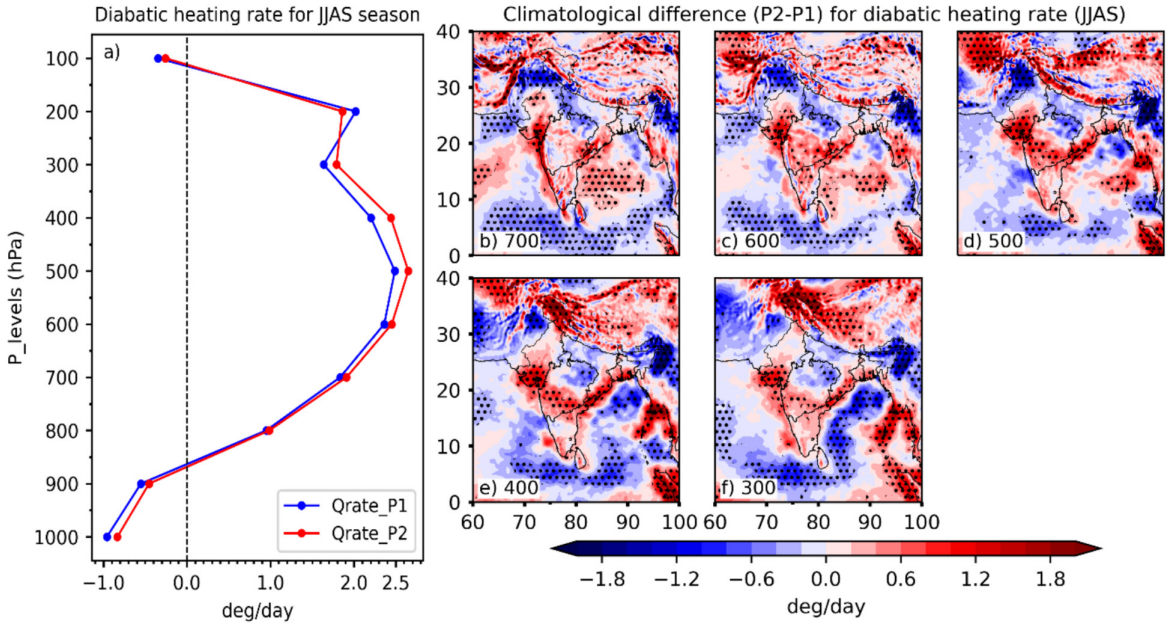

FIGURE 8 | (a) The diabatic heating (Q_1 following Yanai et al. 1973) profile averaged over all India for P1 and P2 and the differences in the diabatic heating at pressure levels of (b) 700, (c) 600, (d) 500, (e) 400 and (f) 300 hPa. The units are in deg/day. The stippled regions in (b–f) indicate significance at the 5% significance level following Student's *t*-test. [Colour figure can be viewed at wileyonlinelibrary.com]

the trends are rising (Figure S10). The difference in total precipitation between P2 and P1 in Figure S11d is a combination of the corresponding differences in the stratiform (Figure 7d) and convective (Figure S10d), respectively.

At higher pressure levels (900–1000 hPa), the correlations in Table 1 become negative and albeit weaker. At higher pressure levels, evaporative flux from the warmer oceans under the prevailing southwesterlies leads to a greater buildup of the moist entropy

in the boundary layer, triggering and sustaining terrestrial monsoonal convection (Ma et al. 2019), which could possibly explain the negative correlations of the thermal contrast with Q_u^r in the P1 period (Table 1). Interestingly, these correlations become weaker in the P2 period, which could be the result of the decreasing trend of convective precipitation over the oceans and NEI in P2 relative to P1 (Figure S10). These weak correlations in Table 1 suggest a weakening relationship of the RC of the moisture flux with the land–ocean thermal contrast in the middle and lower troposphere.

3.4 | Divergent Component of Moisture Flux

Figure 9 illustrates the seasonal climatology of the DC of moisture flux during the JJAS season for the entire period, including P1 and P2. In JJAS, all IHRRs display a strong moisture convergence in the lower troposphere (Figure 9a). In comparison to the lower troposphere (Figure 9a), the DC of moisture flux in the middle troposphere in JJAS is more discontinuous, with CNEI and NWI regions exhibiting moisture divergence amidst moisture convergence in other IHRRs (Figure 9b). In the upper troposphere, however, the DC of moisture flux is largely divergent (Figure 9c).

The convergence and divergence of moisture flux vectors in Figure 9 are construed as moisture sink and source, respectively. The moisture source for the ISMR rainfall from Figure 9a,b is the Arabian Sea, the Indian Ocean to the south of the equator and the Bay of Bengal. However, the Bay of Bengal is the weakest of these in terms of moisture sources, corroborating previous studies (e.g., Pathak et al. 2017; Roxy et al. 2017).

Figure 10 illustrates the changes between the two epochs (P2 − P1) in the climatological seasonal mean DC of moisture flux for the JJAS season. During the JJAS season, the moisture source in the lower troposphere (Figure 10a) just north of the equatorial Indian Ocean is enhanced, while the moisture sink is enhanced over the Indian Ocean south of the equator. Interestingly, Gokul et al. (2024) report that the anomalous changes at sub-seasonal scales in the low-level cloud fraction of the Mascarene High, south of the equator, are precursors to changes in moisture flux convergence in the monsoon trough region at sub-seasonal scales. This leads us to speculate that an increased moisture sink on these decadal scales could be a reflection of the enhancement of low-level cloud fraction over the Mascarene High that could eventually be related to a sustained increased strengthening of the ISM. Furthermore, in JJAS, this sinking is extended over NWI, CI and PNI parts of the Indian landmass, which possibly results in increased rainfall over these regions (Figure 10a). In most other regions and atmospheric layers, the differences in the DC of moisture fluxes are relatively incoherent spatially (Figure 10b,c).

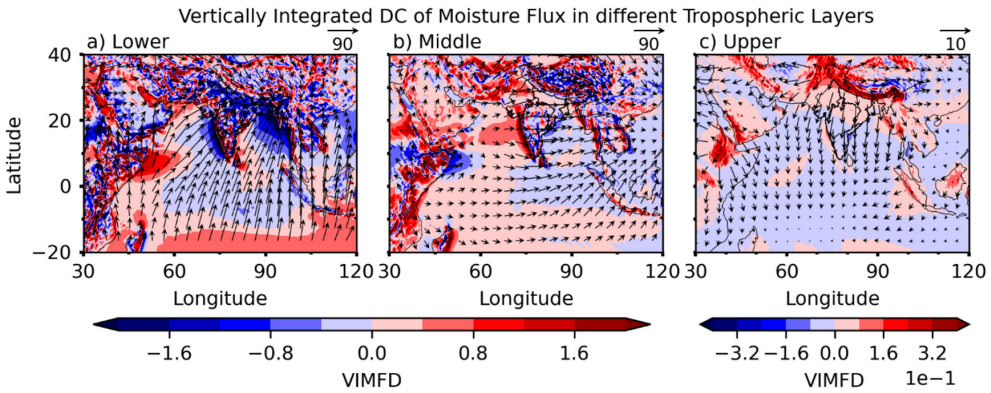

FIGURE 9 | The mean JJAS seasonal climatology (computed over the entire period including periods P1 and P2) of the divergent component of moisture flux (10^{-4} kgm^{-2}s^{-1}; shaded) overlaid with the corresponding divergent moisture flux vectors (kgm^{-1}s^{-1}) in (a) lower (1000–850 hPa), (b) middle (850–500 hPa) and (c) upper (500–100 hPa) layers of the troposphere. [Colour figure can be viewed at wileyonlinelibrary.com]

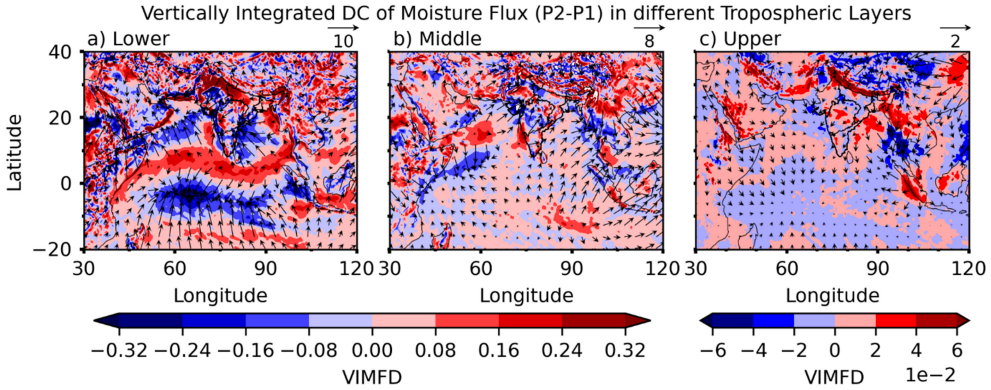

FIGURE 10 | The JJAS seasonal climatological change (P2 − P1) of the divergent component of moisture flux (10^{-4} kgm^{-2}s^{-1}; shaded) overlaid with corresponding changes in divergent moisture flux vectors (kgm^{-1}s^{-1}) in (a) lower (1000–850 hPa), (b) middle (850–500 hPa) and (c) upper (500–100 hPa) layers of the troposphere. [Colour figure can be viewed at wileyonlinelibrary.com]

The mean differences in evaporation and precipitation between the two epochs (P2 – P1) for JJAS are shown in Figure S12. The regions of moisture convergence and divergence in the lower troposphere in Figure 10 are coincident with negative (moisture sink) and positive (moisture source) values of the mean difference between evaporation and precipitation fields in Figure S12, respectively. For example, the surplus mean rainfall over NWI, CI and PNI and a deficit of over NEI and the western CNEI in the JJAS season (Figure S12b) are nearly coincident with corresponding moisture flux convergence and divergence in the lower troposphere, respectively (Figure 10a).

3.5 | Analysis of Rainfall

In order to further analyse the impact of the changes mentioned above in moisture flux components between the two epochs, we examined the corresponding changes in the linear trends of the mean JJAS rainfall (Figure S13). In the recent epoch (P2), a strong positive trend ranging up to 2 mm day^{-1} decade^{-1}, with a statistical significance level of 5%, is observed for all IHRRs except the western and eastern flanks of CNEI and the NEI, where a declining trend of up to 2mm day^{-1} decade^{-1} is observed (Figure S13b). The strongest trend is seen over parts of NWI and CI in P2 (Figure S13b). At the all India average level, in P1, an insignificant negative trend of −0.064 mm^{-1}decade^{-1} is observed in the JJAS mean rainfall (Figure S13c). However, in P2, contrary to P1, a statistically significant positive trend of the all India average of mean JJAS rainfall of 0.3 mm day^{-1} decade^{-1} is seen (Figure S13c). However, compared to the trends shown in Figure S13a,b, the temporal trend of rainfall averaged over all of India seems to be diluted due to a strong positive trend over NWI, CI and PNI with a negative trend over CNEI and NEI. Similarly, Jin and Wang (2017) have reported a positive trend in ISMR (measured as area averaged over CI) since 2002 using multiple observational/reanalysis datasets.

4 | Conclusion

The study provides a unique perspective to the rising trend of the PWC in the recent decades (2002–2021; P2) relative to prior decades (1959–2001; P2) of the ISMR. We analyse these changes in the lower (1000–850 hPa), middle (850–500 hPa) and upper (500–100 hPa) troposphere separately. The analysis included examining changes in moisture flux patterns which were partitioned into their RCs and DCs that inform on the moisture transport and moisture source/sink, respectively. We also examined changes in precipitation between the two periods and their partitioning between convective and stratiform precipitation. Such analysis in the context of the current revival of the ISM is unique to this study.

The linear trends of PWC are observed to increase significantly in the recent P2 period relative to P1 over most of India during JJAS, with some exceptions over parts of northwest and hilly regions of India. In fact, the trends of the all India mean JJAS PWC over India in P2 become statistically significant at the 10% significance level in contrast to the statistically insignificant trends in the P1 period. The pre-monsoon season of MAM exhibits a similar change but is smaller in magnitude in the linear trends of PWC and over a limited region confined to northwest India. The largest seasonal mean JJAS of PWC between P2 and P1 is observed in the middle troposphere with associated large changes in the RC of the moisture flux, which suggests an enhancement of the cross-equatorial southwesterly moisture flux of the ISM in P2. This enhancement of the RC of the moisture flux in the middle troposphere is also accompanied by increased land–ocean thermal contrast and an increase in the fraction of stratiform precipitation of the ISMR in P2 relative to P1. We suggest that this latter change has a profound influence on enhancing the mid-tropospheric moisture flux and also on weakening its relationship with land–ocean thermal contrast.

The seasonal climatology of the DC of moisture flux in the JJAS season shows a moisture sink over IHHRs with deep convection over CI, PNI and NEI, except for CNEI and some parts of NWI. The seasonal climatology of the moisture divergence (source) is observed over the Arabian Sea and over the equatorial Indian Ocean. The recent changes (P2 – P1) in the DC of the moisture flux reveal that the tropical Indian Ocean just north of the equator serves as a large moisture source for the strengthened (weakened) moisture sink over the equatorial Indian Ocean and the NWI, CI and PNI (CNEI and NEI) which, in turn, result in increased (decreased) rainfall trends over these regions.

The attribution of the current revival of the ISM is a challenging task. It appears that the changing land–ocean thermal contrast is a result of changing greenhouse gas concentrations, which result in the mid-tropospheric changes observed in this study. However, it would be more conclusive by conducting specialised modelling experiments that examine the sensitivity of these changes of the ISM to radiative forcing from changing greenhouse concentrations.

Author Contributions

Amarjeet: conceptualization, methodology, software, validation, formal analysis, investigation, resources, data curation, writing – original draft, visualization. **Vasubandhu Misra:** writing – review and editing, investigation. **Arun Chakraborty:** conceptualization, investigation, writing – review and editing, supervision. **Anil K. Gupta:** conceptualization, investigation, writing – review and editing, supervision. **Vineet Sharma:** conceptualization, methodology, data curation.

Acknowledgements

Amarjeet acknowledges the INSPIRE Division, Department of Science and Technology (DST), Government of India, for providing fellowship (IF190627) to conduct the research at IIT Kharagpur. The HPC Paramshakti facility of IIT Kharagpur is greatly acknowledged. A.K.G. thanks the Anusandhan National Research Foundation (ANRF), New Delhi, for financial support under the J.C. Bose Fellowship (Grant JBR/2021/000019). A.C. gratefully acknowledges the financial support given by the Indian Institute of Tropical Meteorology Pune, Ministry of Earth Sciences, Government of India to conduct this research under Monsoon Mission III (Grant IITM/MM-III/2024/AI-P06/SO-006). We are thankful to the anonymous reviewers for their valuable comments and suggestions that helped to improve the standard of the manuscript.

Conflicts of Interest

The authors declare no conflicts of interest.

Data Availability Statement

The ERA-5 and IMD datasets are available at the Copernicus Climate Change Service's Climate Data Store (https://cds.climate.copernicus.eu/cdsapp; Hersbach et al. 2019) and IMD website (https://www.imdpune.gov.in/cmpg/Griddata/Rainfall_25_Bin.html; Kishore et al. 2016), respectively. The IGRA data are downloaded from the NCEI-NOAA website (https://www.ncei.noaa.gov/products/weather-balloon/integrated-global-radiosonde-archive). All figures are generated using the Jupyter Notebook interface of the IPython Interactive Project (https://ipython.org/; Pérez and Granger 2007).

References

Amarjeet, S., V. Sharma, C. P. Pandey, A. K. Gupta, and A. Chakraborty. 2023. "Study of Moisture Flux Over Uttarakhand State: Signature of Cloud Bursts." *Climate Dynamics* 61: 5349–5366.

Asoka, A., T. Gleeson, Y. Wada, and V. Mishra. 2017. "Relative Contribution of Monsoon Precipitation and Pumping to Changes in Groundwater Storage in India." *Nature Geoscience* 10, no. 2: 109–117.

Bengtsson, L., K. Hodges, and S. Hagemann. 2004. "Sensitivity of Large-Scale Atmospheric Analyses to Humidity Observations and Its Impact on the Global Water Cycle and Tropical and Extratropical Weather Systems in ERA40." *Tellus* 56A: 202–217.

Bollasina, M. A., Y. Ming, V. Ramaswamy, M. D. Schwarzkopf, and V. Naik. 2014. "Contribution of Local and Remote Anthropogenic Aerosols to the Twentieth Century Weakening of the South Asian Monsoon." *Geophysical Research Letters* 41, no. 2: 680–687.

Chakraborty, A., S. K. Behera, M. Mujumdar, R. Ohba, and T. Yamagata. 2006. "Diagnosis of Tropospheric Moisture Over Saudi Arabia and Influences of IOD and ENSO." *Monthly Weather Review* 134: 598–617.

Choudhury, A. D., and R. Krishnan. 2011. "Dynamical Response of the South Asian Monsoon Trough to Latent Heating From Stratiform and Convective Precipitation." *Journal of the Atmospheric Sciences* 68, no. 6: 1347–1363.

Durre, I., R. S. Vose, and D. B. Wuertz. 2006. "Overview of the Integrated Global Radiosonde Archive." *Journal of Climate* 19, no. 1: 53–68.

Durre, I., X. Yin, R. S. Vose, S. Applequist, and J. Arnfield. 2018. "Enhancing the Data Coverage in the Integrated Global Radiosonde Archive." *Journal of Atmospheric and Oceanic Technology* 35, no. 9: 1753–1770.

Gadgil, S., Y. P. Abrol, and P. S. Rao. 1999. "On Growth and Fluctuation of Indian Foodgrain Production." *Current Science* 76: 548–556.

Gokul, T., R. K. Vellore, D. C. Ayantika, V. Divya, R. Krishnan, and M. J. K. Reji. 2024. "Low Clouds Over the Subtropical Indian Ocean and Sub-Seasonal Circulation Associations With the Indian Summer Monsoon." *Climate Dynamics* 62: 2069–2106.

Haltiner, G. J., and R. T. Williams. 1980. *Numerical Prediction and Dynamic Meteorology*. Wiley.

Hersbach, H., B. Bell, P. Berrisford, et al. 2019. "ERA5 Monthly Averaged Data on Pressure Levels From 1959 to Present. Copernicus Climate Change Service (C3S) Climate Data Store (CDS)." https://doi.org/10.24381/cds.6860a573.

Hirsch, R. M., and J. R. Slack. 1984. "A Nonparametric Trend Test for Seasonal Data With Serial Dependence." *Water Resources Research* 20, no. 6: 727–732. https://doi.org/10.1029/WR020i006p00727.

Houze, R. A., Jr. 2004. "Mesoscale Convective Systems." *Reviews of Geophysics* 42, no. 4: 1–43.

Jin, Q., and C. Wang. 2017. "A Revival of Indian Summer Monsoon Rainfall Since 2002." *Nature Climate Change* 7, no. 8: 587–594.

Kishore, P., S. Jyothi, G. Basha, et al. 2016. "Precipitation Climatology Over India: Validation With Observations and Reanalysis Datasets and Spatial Trends." *Climate Dynamics* 46: 541–556.

Krishnamurti, T. N., H. S. Bedi, V. Hardiker, and L. Watson-Ramaswamy. 2006. *An Introduction to Global Spectral Modeling*. Vol. 35. Springer Science & Business Media.

Krishnan, R., K. Vishisth, D. C. Ayantika, K. M. Sumit, and R. Vellore. 2025. "Climate Change and Monsoon Rainstorms." In *Anatomy, Early Warning Systems and Aftermath in Changing Climate Scenarios*, edited by S. Severe, 545–562. Springer Nature Singapore.

Kumar, S., A. Chakraborty, R. Chandrakar, A. Kumar, B. Sadhukhan, and R. Roy Chowdhury. 2023. "Analysis of Marine Heatwaves Over the Bay of Bengal During 1982–2021." *Scientific Reports* 13, no. 1: 14235.

Kumari, A., P. Kumar, A. K. Dubey, A. K. Mishra, and M. S. Saharwardi. 2022. "Dynamical and Thermodynamical Aspects of Precipitation Events Over India." *International Journal of Climatology* 42, no. 5: 3094–3106.

Ma, D., A. H. Sobel, Z. Kuang, M. S. Singh, and J. Nie. 2019. "A Moist Entropy Budget View of the South Asian Summer Monsoon Onset." *Geophysical Research Letters* 46, no. 8: 4476–4484.

Mapes, B. E. 1993. "Gregarious Tropical Convection." *Journal of Atmospheric Sciences* 50, no. 13: 2026–2037.

Misra, V., P. Pantina, C. Chan, and S. DiNapoli. 2012. "A Comparative Study of the Indian Summer Monsoon Hydroclimate and Its Variations in Three Reanalyses." *Climate Dynamics* 39: 1149–1168.

Mooley, D. A., and B. Parthasarathy. 1984. "Fluctuations in All-India Summer Monsoon Rainfall During 1871–1978." *Climatic Change* 6, no. 3: 287–301.

Noska, R., and V. Misra. 2016. "Characterizing the Onset and Demise of the Indian Summer Monsoon." *Geophysical Research Letters* 43, no. 9: 4547–4554.

Parthasarathy, B., K. Rupa Kumar, and A. A. Munot. 1996. *Homogeneous Regional Summer Monsoon Rainfall Over India: Interannual Variability and Teleconnections*. Research Report 65 (RR-65). Indian Institute of Tropical Meteorology, Pune.

Patel, V. K., and J. Kuttippurath. 2022. "Significant Increase in Water Vapour Over India and Indian Ocean: Implications for Tropospheric Warming and Regional Climate Forcing." *Science of the Total Environment* 838: 155885.

Pathak, A., S. Ghosh, and P. Kumar. 2014. "Precipitation Recycling in the Indian Subcontinent During Summer Monsoon." *Journal of Hydrometeorology* 15, no. 5: 2050–2066.

Pathak, A., S. Ghosh, J. A. Martinez, F. Dominguez, and P. Kumar. 2017. "Role of Oceanic and Land Moisture Sources and Transport in the Seasonal and Interannual Variability of Summer Monsoon in India." *Journal of Climate* 30: 1839–1859.

Pérez, F., and B. E. Granger. 2007. "IPython: A System for Interactive Scientific Computing." *Computing in Science & Engineering* 9, no. 3: 21–29.

Ramesh Kumar, M. R., S. S. C. Shenoi, and P. Schluessel. 1999. "On the Role of the Cross Equatorial Flow on Summer Monsoon Rainfall Over India Using NCEP/NCAR Reanalysis Data." *Meteorology and Atmospheric Physics* 70, no. 3: 201–213.

Ratna, S. B., A. Cherchi, P. V. Joseph, S. Behera, B. Abish, and S. Masina. 2014. *Moisture Trend Over the Arabian Sea and Its Influence on the Indian Summer Monsoon Rainfall*. CMCC Research Paper (RP0225).

Rosen, R. D., D. A. Salstein, and J. Peixoto. 1979. "Streamfunction Analysis of Interannual Variability in Large-Scale Water Vapor Flux." *Monthly Weather Review* 107, no. 12: 1682–1684.

Roxy, M. K. 2017. "Land Warming Revives Monsoon." *Nature Climate Change* 7, no. 8: 549–550.

Roxy, M. K., S. Ghosh, A. Pathak, et al. 2017. "A Threefold Rise in Widespread Extreme Rain Events Over Central India." *Nature Communications* 8, no. 1: 708.

Roxy, M. K., K. Ritika, P. Terray, R. Murtugudde, K. Ashok, and B. N. Goswami. 2015. "Drying of Indian Subcontinent by Rapid Indian Ocean Warming and Weakening Land–Sea Thermal Gradient." *Nature Communications* 6, no. 7423: 1–10. https://doi.org/10.1038/ncom.

Ruprecht, E., and T. Kahl. 2003. "Investigation of the Atmospheric Water Budget of the BALTEX Area Using NCEP/NCAR Reanalysis Data." *Tellus A: Dynamic Meteorology and Oceanography* 55: 426–437.

Sarkar, S., J. Kuttippurath, and V. K. Patel. 2023. "Long-Term Changes in Precipitable Water Vapour Over India Derived From Satellite and Reanalysis Data for the Past Four Decades (1980–2020)." *Environmental Science: Atmospheres* 3, no. 4: 749–759.

Schumacher, C., R. A. Houze Jr., and I. Kraucunas. 2004. "The Tropical Dynamical Response to Latent Heating Estimates Derived From the TRMM Precipitation Radar." *Journal of the Atmospheric Sciences* 61, no. 12: 1341–1358.

Sharma, V., Amarjeet, S. Sharma, and A. Chakraborty. 2024. "Evidence of Strengthening of Tropical Easterly Jet After 1998 Climate Shift Using ERA-5 Datasets." *Theoretical and Applied Climatology* 155: 5859–5874.

Singh, D., S. Gosh, and M. K. Roxy. 2019. "Indian Summer Monsoon: Extreme Events, Historical Changes and Role of Anthropogenic Forcings." *Wiley Interdisciplinary Reviews: Climate Change* 10, no. 2: e571.

Tomar, C. S., R. Bhatla, N. L. Singh, et al. 2024. "Evaluation of Atmospheric Precipitable Water Vapour Distribution and Trend Over India." *Theoretical and Applied Climatology* 155, no. 8: 8361–8377.

Trenberth, K. E., J. Fasullo, and L. Smith. 2005. "Trends and Variability in Column Integrated Atmospheric Water Vapor." *Climate Dynamics* 24: 741–758.

Trenberth, K. E., J. T. Fasullo, and J. Mackaro. 2011. "Atmospheric Moisture Transports From Ocean to Land and Global Energy Flows in Reanalyses." *Journal of Climate* 24, no. 18: 4907–4924.

Ullah, K., and S. Gao. 2012. "Moisture Transport Over the Arabian Sea Associated With Summer Rainfall Over Pakistan in 1994 and 2002." *Advances in Atmospheric Sciences* 29: 501–508.

Yanai, M., S. Esbensen, and J. H. Chu. 1973. "Determination of Bulk Properties of Tropical Cloud Clusters From Large-Scale Heat and Moisture Budgets." *Journal of Atmospheric Sciences* 30, no. 4: 611–627.

Yanai, M., C. Li, and Z. Song. 1992. "Seasonal Heating of the Tibetan Plateau and Its Effects on the Evolution of the Asian Summer Monsoon." *Journal of the Meteorological Society of Japan. Ser. II* 70, no. 1: 319–351.

Supporting Information

Additional supporting information can be found online in the Supporting Information section.

Supplementary Material

A Study of Recent Changes in Moisture Flux Patterns over India: Implications for Indian Summer Monsoon Rainfall

Amarjeet[1], Vasubandhu Misra[2, 3], Arun Chakraborty[1, *], Anil K. Gupta[4], Vineet Sharma[1]

[1]Centre for Ocean, River, Atmosphere and Land Sciences (CORAL), Indian Institute of Technology Kharagpur, Kharagpur, WB, India.
[2]Centre for Ocean-Atmospheric Prediction Studies (COAPS), Florida State University, Tallahassee, FL, USA.
[3]Department of Earth, Ocean and Atmospheric Science, Florida State University, Tallahassee, FL, USA.
[4]Department of Geology and Geophysics, Indian Institute of Technology Kharagpur, Kharagpur, WB, India.

*Corresponding Author: arunc@coral.iitkgp.ac.in

Contents of this file

Figures S1 to S13

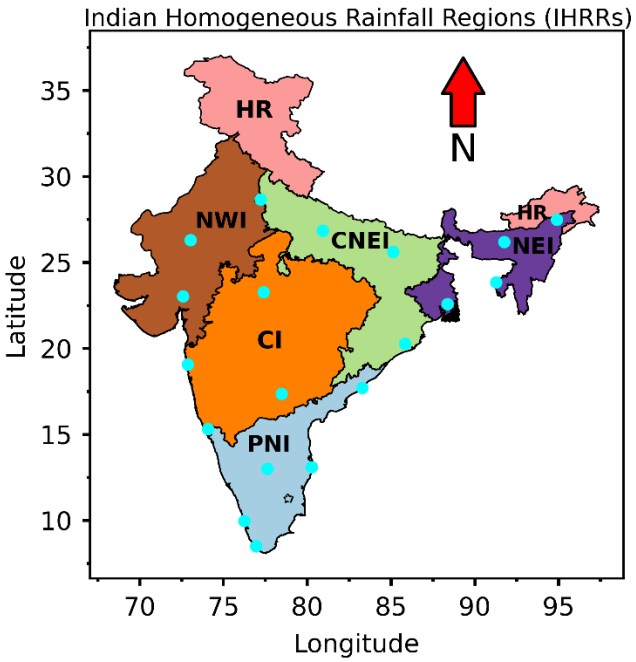

Figure S1: Indian homogeneous rainfall regions (IHRRs): North-Western India (NWI), Central North-Eastern India (CNEI), North-Eastern India (NEI), Central India (CI), Peninsular India (PNI), and Hilly Regions (HR). The cyan-filled circle shows the 19 locations (Table S1) throughout India for which the IGRA sonde-derived PWC data is obtained to validate the ERA-5 PWC.

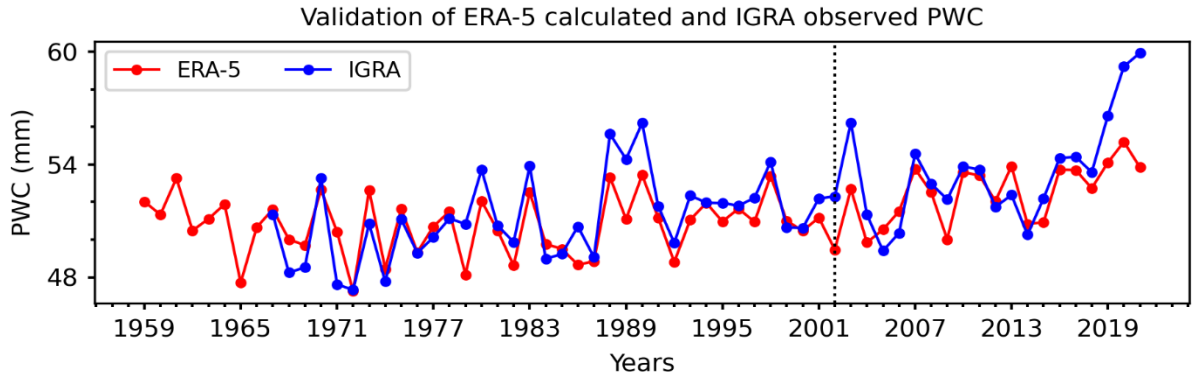

Figure S2: The time series of JJAS mean PWC validation from ERA-5 reanalysis and the corresponding average of sonde observations over 19 locations across India from the Integrated Global Radiosonde Archive (IGRA v2.0).

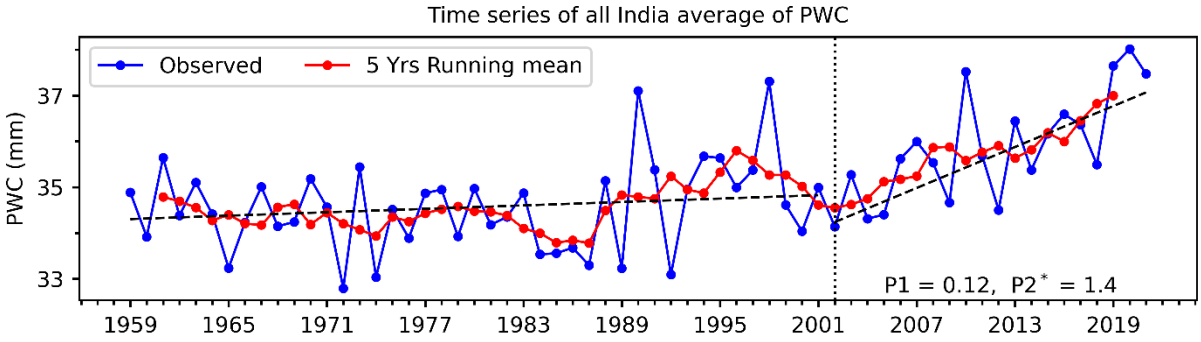

Figure S3: Time series of all India average of annual mean PWC. The legend indicates the slopes of the trends in mm/decade for P1 and P2, where '*' shows significance at 10% significance level following the Mann-Kendall test. The red and black (dashed) lines show the five-year running mean and slope of the trends, respectively.

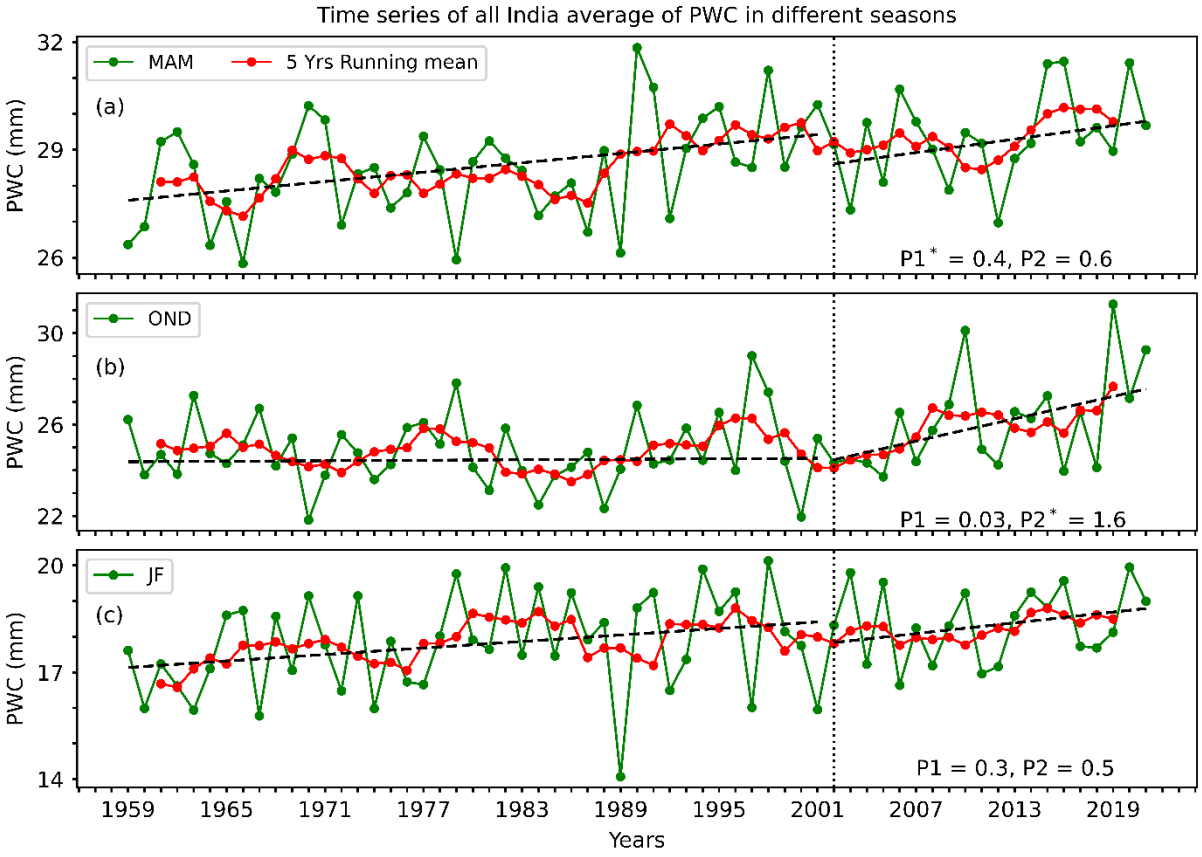

Figure S4: Time series of all India average of mean (a) MAM, (b) OND, and (c) JF PWC. The legend indicates the slopes of the trends in mm/decade for P1 and P2, where '*' shows significance at 10% significance level following the Mann-Kendall test. The red and black (dashed) lines show the five-year running mean and slope of the trends, respectively.

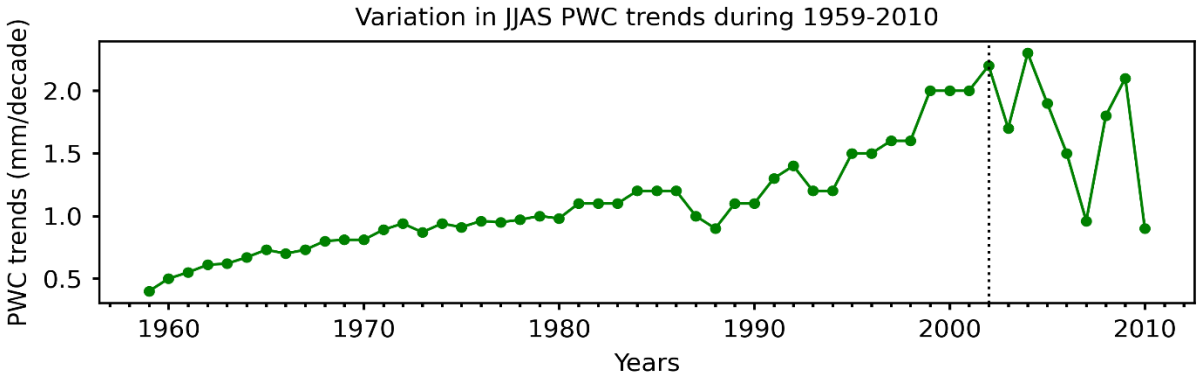

Figure S5: Rolling linear decadal trends of the mean JJAS precipitation over India computed each year from 1959 to 2021. The decadal trends are shown only up to 2010 because of inadequate sample size to compute the trends beyond this year.

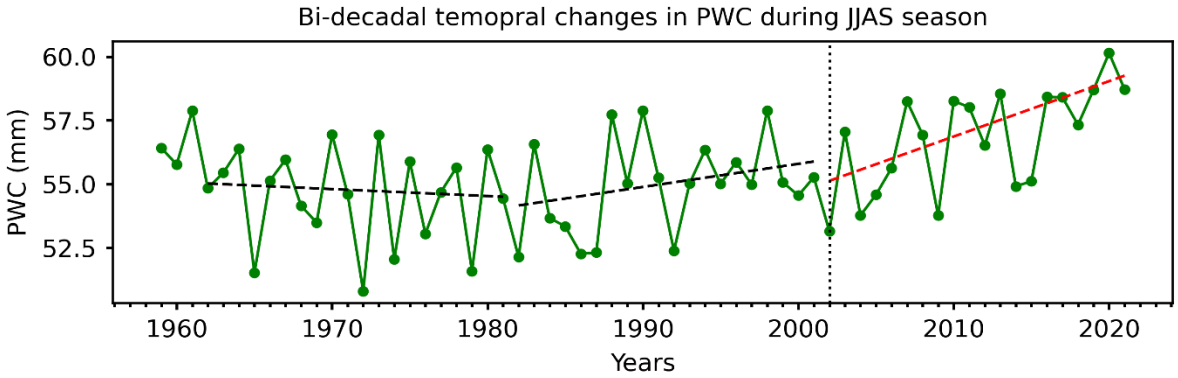

Figure S6: Linear trends for 20-year segments: 1962-1981 (First black dashed line; -0.27 mm/decade), 1982-2001 (Second black dashed line; 0.9 mm/decade), and 2002-2021 (Red dashed line; 2.2 mm/decade). The trend in Segment 3 (2002-2021) is statistically significant at 1% significance level, while the trends in other segments are statistically insignificant.

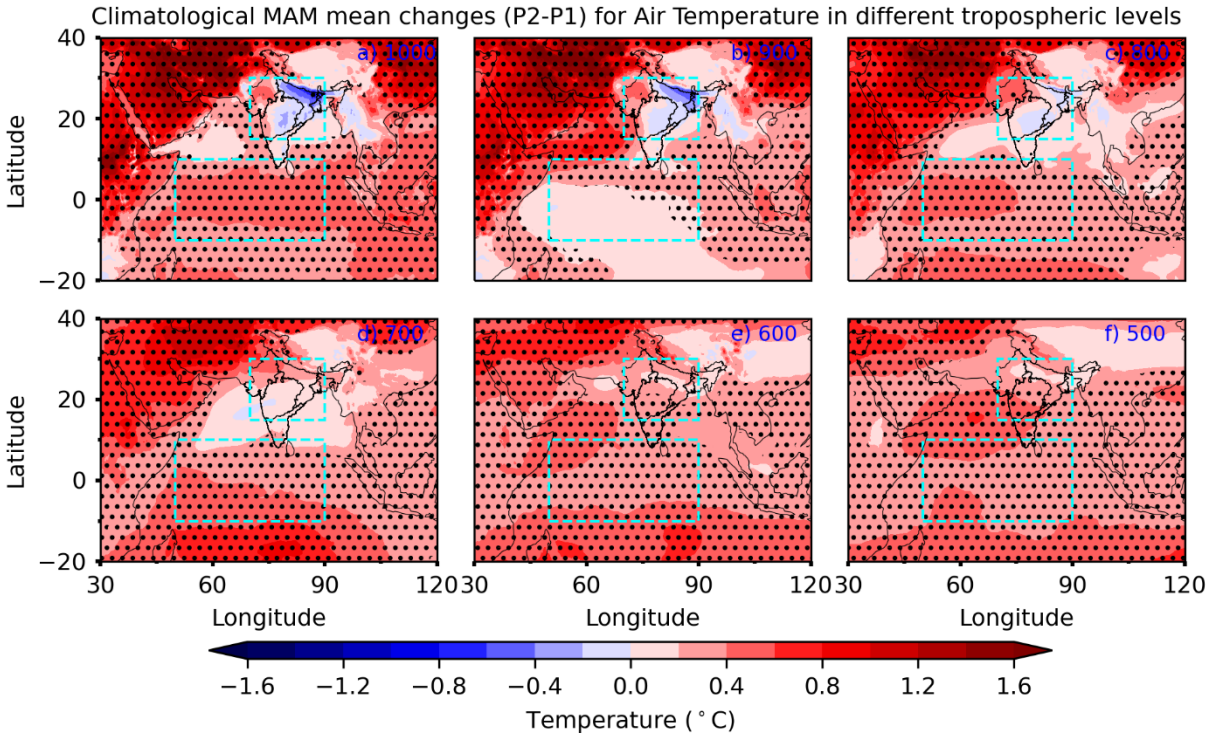

Figure S7: Seasonal mean MAM climatological change (P2-P1) in tropospheric air temperature at a) 1000, b) 900, c) 800, d) 700, e) 600, and f) 500 hPa. The stippled regions show significance at a 5% significance level following the Student's t-test.

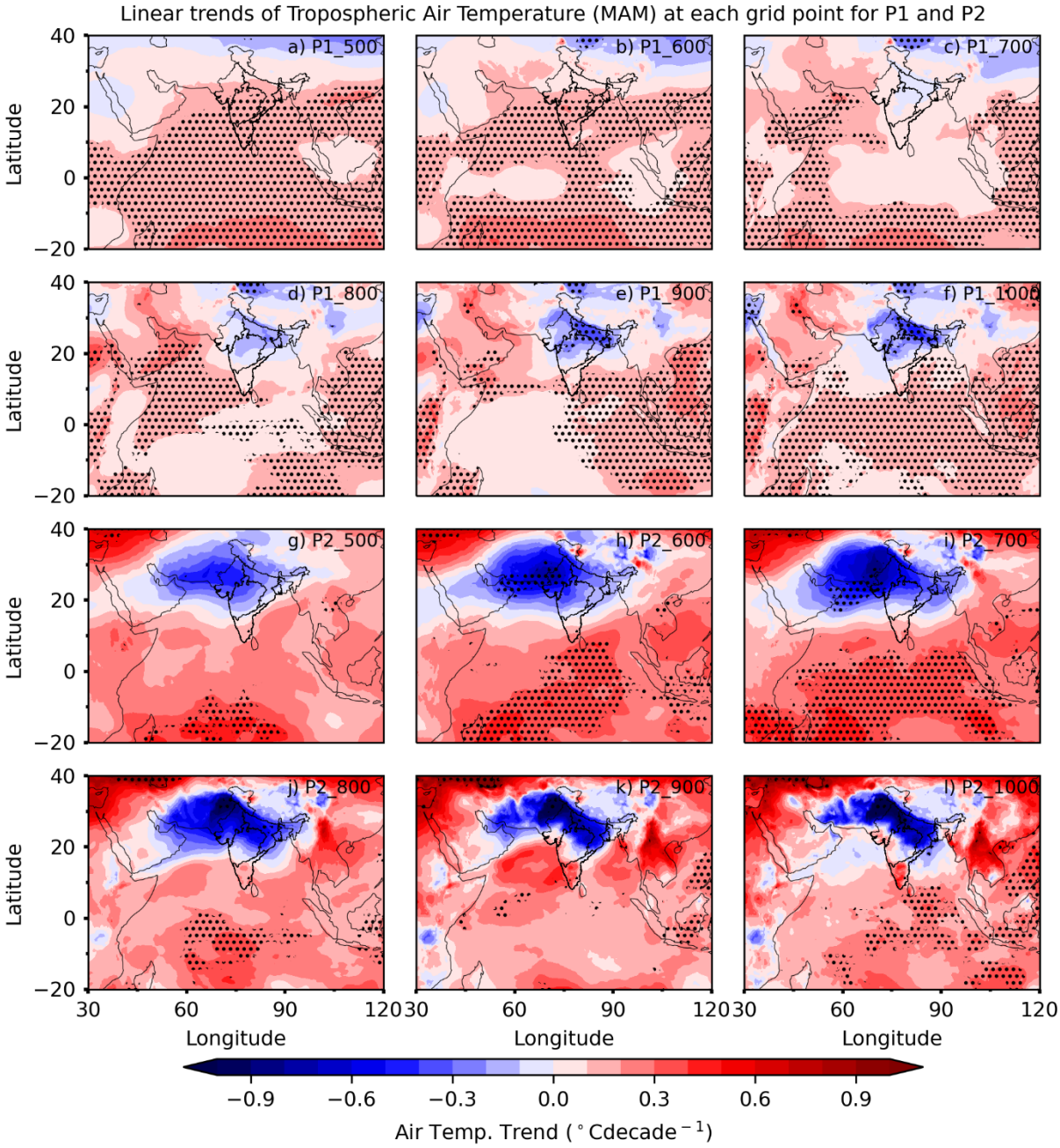

Figure S8: The linear trend of mean MAM tropospheric air temperature at each grid point at (a, g) 500 hPa, (b, h) 600 hPa, (c, i) 700 hPa, (d, j) 800 hPa, (e, k) 900, and (f, l) 1000 hPa for (a-f) P1 and (g-l) P2 periods. The stippled regions indicate significance at 5% significance level according to the Mann-Kendall test.

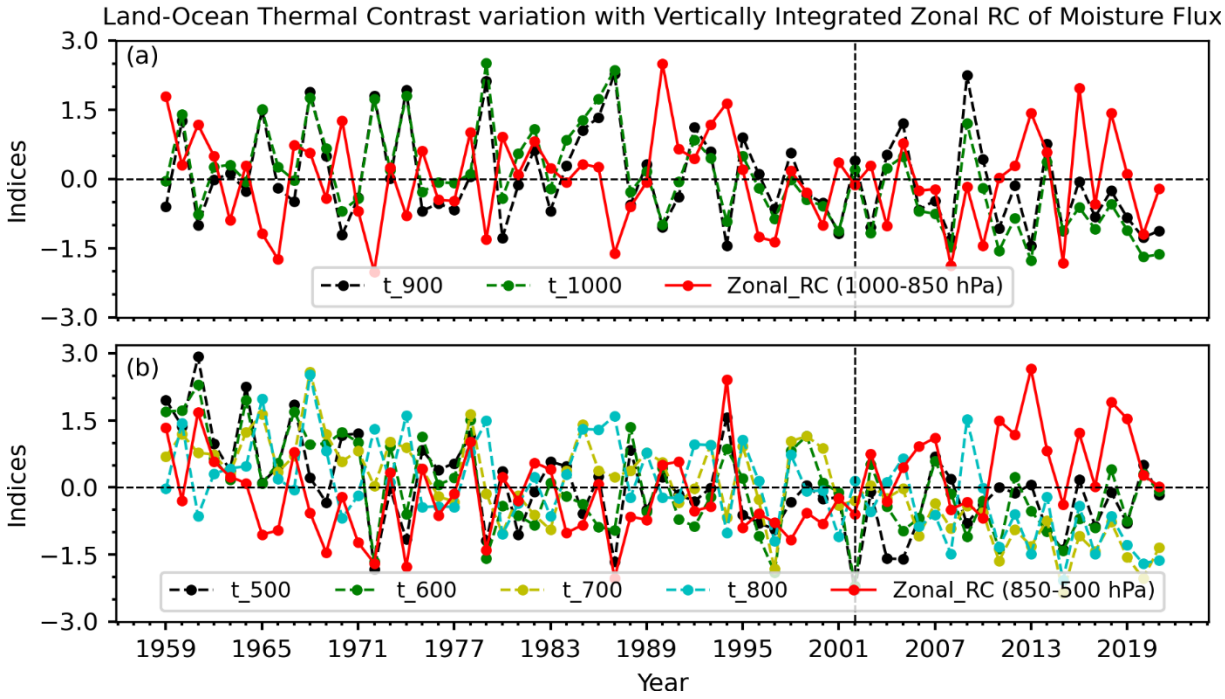

Figure S9: Time series of seasonal mean JJAS land-ocean thermal contrast at (a) 900 and 1000 hPa and (b) 500 – 800 hPa with the vertically integrated zonal rotational component (RC) of moisture flux (Unit: $kgm^{-1}s^{-1}$) in the (a) lower (1000-850 hPa) and (b) middle (850-500 hPa) tropospheric layers.

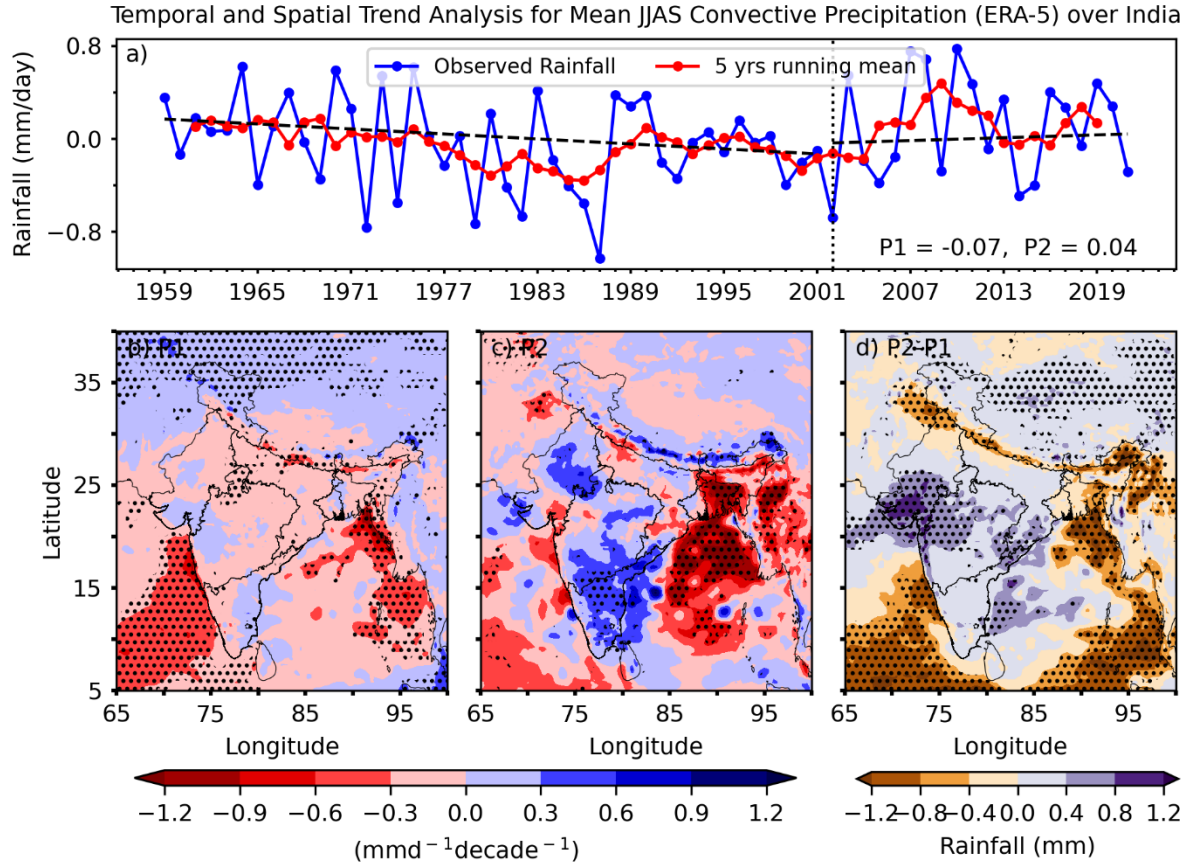

Figure S10: (a) Time series of the mean JJAS all India averaged convective precipitation from ERA5 with the legend indicating the slopes of the trends for P1 and P2 in $mmd^{-1}decade^{-1}$. The red and black (dashed) lines show the five-year running mean and slope of the trends, respectively. The spatial distribution of the linear trends of mean JJAS stratiform precipitation from ERA5 for (b) P1 and (c) P2, and (d) the corresponding differences P2-P1. The stippled regions indicate significance at 5% significance level according to the Mann-Kendall test.

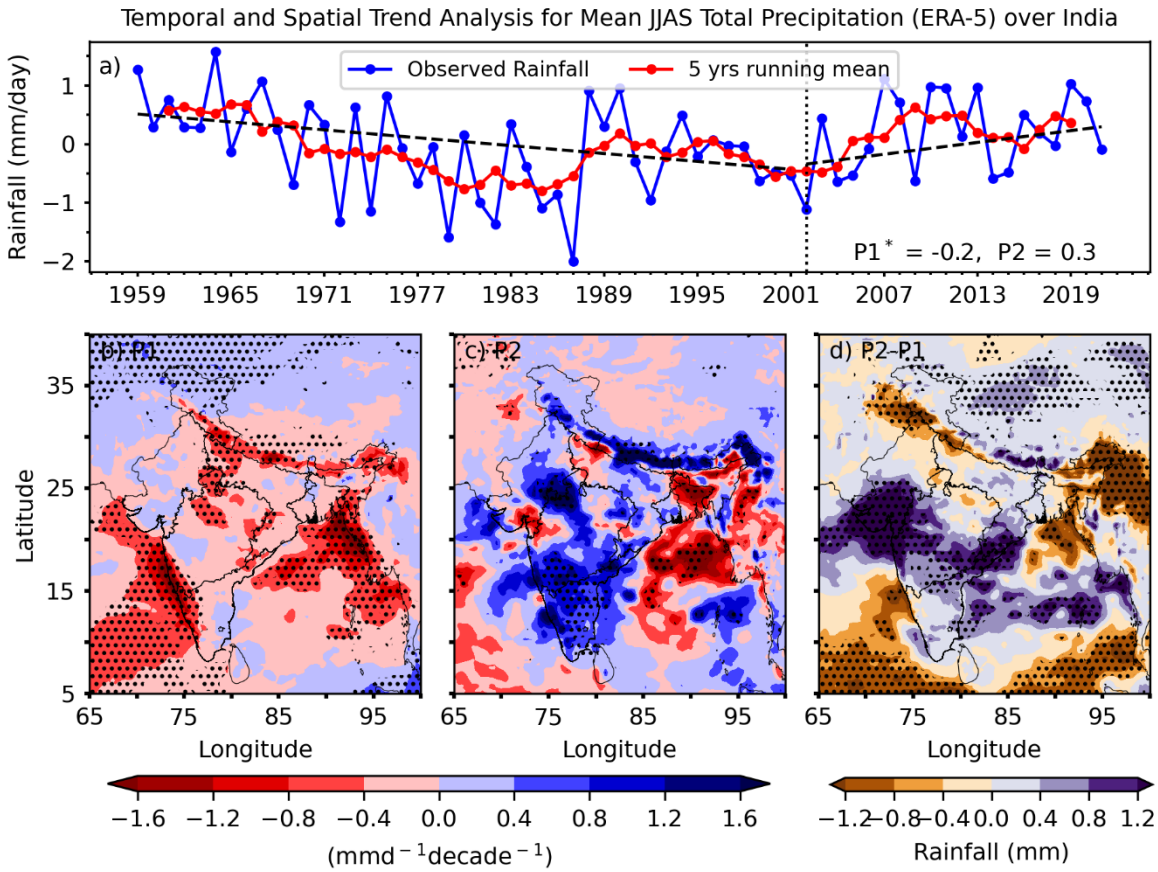

Figure S11: (a) Time series of the mean JJAS all India averaged total precipitation from ERA5 with the legend indicating the slopes of the trends for P1 and P2 in $mmd^{-1}decade^{-1}$, where '*' shows significance at 5% significance level following the Mann-Kendall test. The red and black (dashed) lines show the five-year running mean and slope of the trends, respectively. The spatial distribution of the linear trends of mean JJAS stratiform precipitation from ERA5 for (b) P1 and (c) P2, and (d) the corresponding differences P2-P1. The stippled regions indicate significance at 5% significance level according to the Mann-Kendall test.

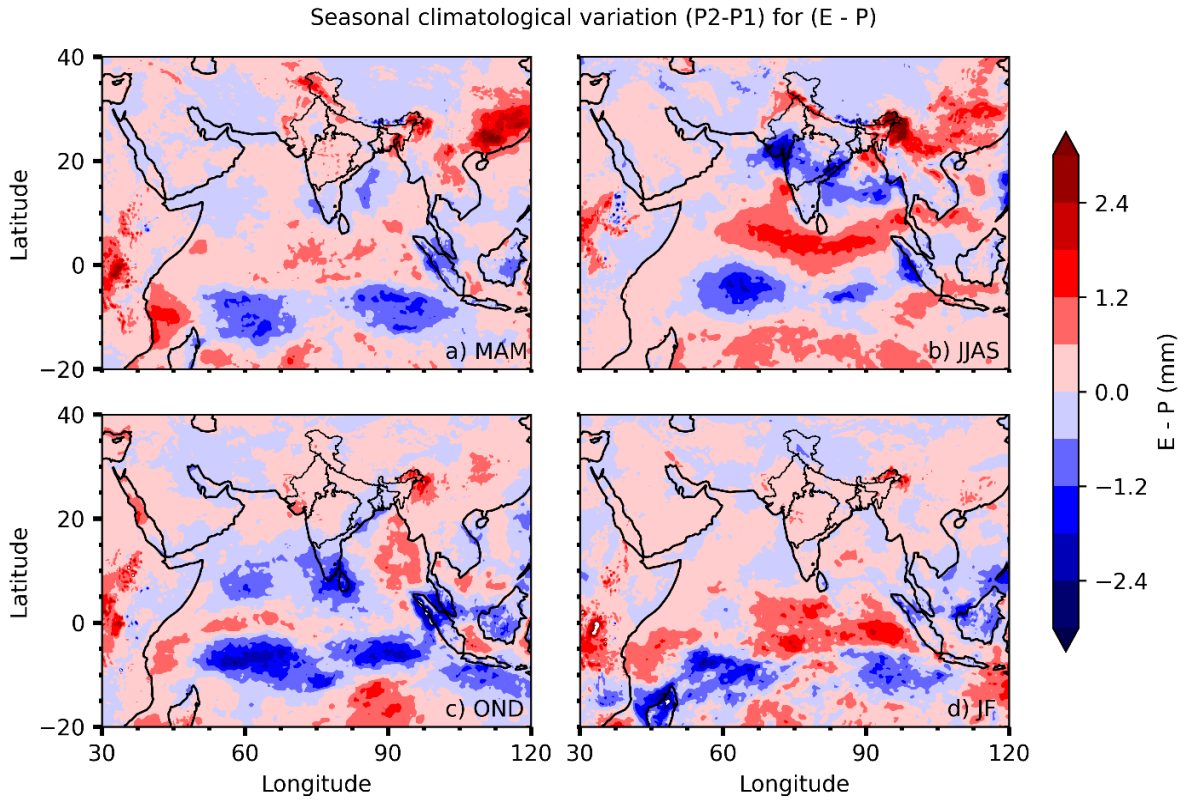

Figure S12: The climatological seasonal mean (a) MAM, (b) JJAS, (c) OND, and (d) JF difference of evaporation and precipitation (E-P) for P2 - P1.

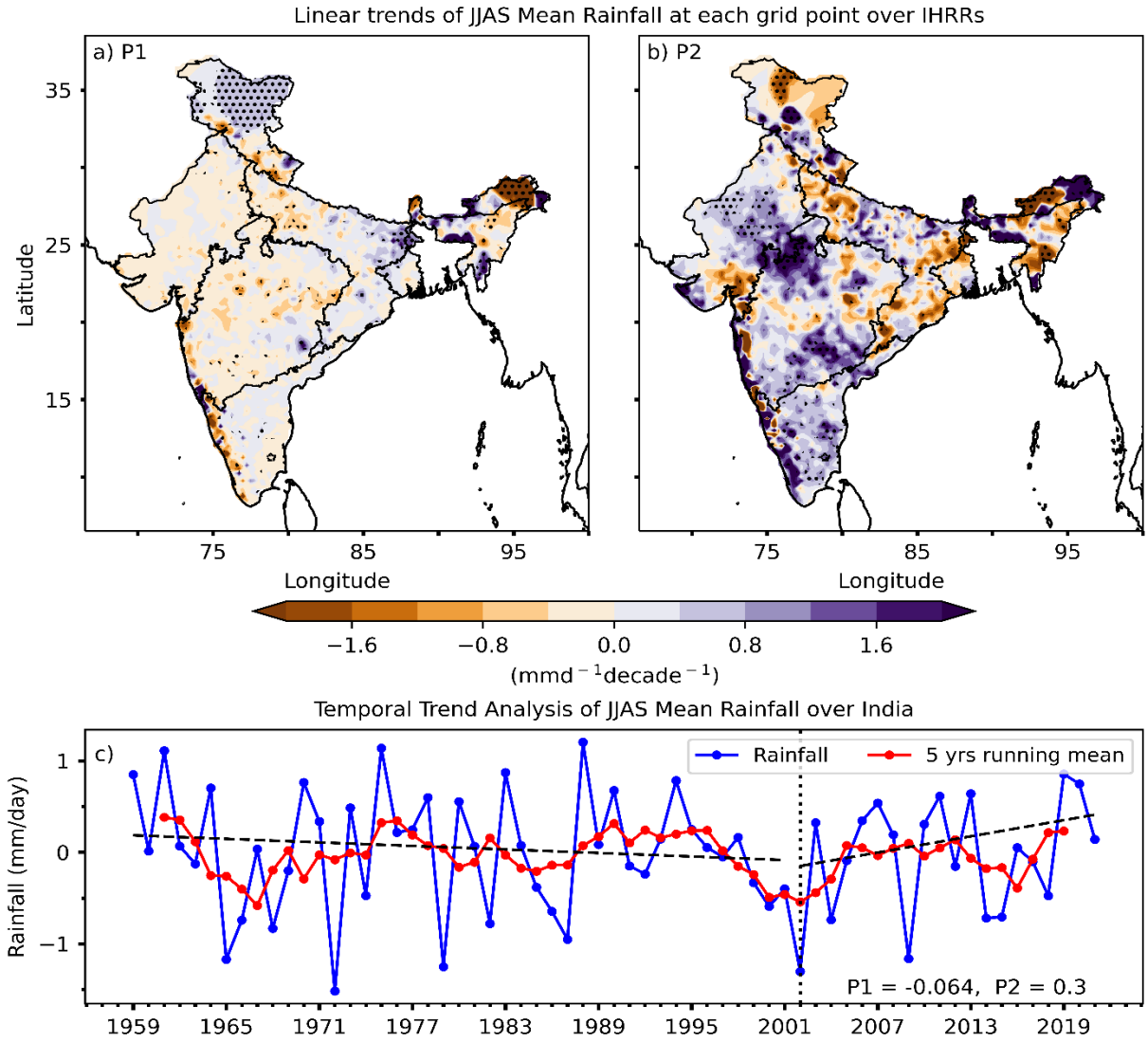

Figure S13: The linear trends of the mean JJAS rainfall at each grid point over IHRRs for (a) P1 and (b) P2. The stippled regions show significance at 5% significance level following the Mann-Kendall test. (c) Temporal trend analysis of JJAS rainfall over IHRRs (India). The legend indicates the slopes of the trends in mm/decade for P1 and P2. The red and black (dashed) lines show the five-year running mean and slope of the trends, respectively.

Table S1: List locations for which the PWC data is obtained from the Integrated Global Radiosonde Archive (IGRA v2.0) provided by NCEI-NOAA.

Serial No.	City Name	Data Availability Period
1	Ahmedabad	1967-2021
2	Jodhpur	1967-2021
3	Mumbai	1967-2020
4	Cochin	1988-2021
5	Thiruvananthapuram	1969-2020
6	Chennai	1967-2021
7	Visakhapatnam	1967-2021
8	Hyderabad	1971-2002
9	Bhopal	1983-2021
10	Bhubaneswar	1971-2021
11	Guwahati	1967-2021

12	Kolkata	1967-2020
13	Patna	1983-2020
14	Agartala	1978-2021
15	Dibrugarh	1978-2021
16	Lucknow	1967-2020
17	New Delhi	1966-2021
18	Bengaluru	1961-2020
19	Goa/Panji	1971-2021